Applications of a two-way debonding theory to short fibre composites

C.K.Y. LEUNG and V.C. LI

(Massachusetts Institute of Technology, USA)

Traditional fibre debonding theories which consider debonding only from the loaded end of the fibre are only applicable to composites with low fibre volume fraction, low fibre/matrix moduli ratio and high interfacial strength/interfacial friction ratio. A two-way debonding theory, which is applicable to all general cases, has recently been developed. In this paper, major findings from the new two-way theory are first summarized. The new theory is compared with traditional theories with respect to the prediction of composite properties. For the fibre pull-out test specimen, where fibre volume fraction is very low, a new method of deriving interfacial bond properties based on one-way debonding theory is presented. For practical composite systems, the significance of employing the new two-way debonding theory is discussed.

Key words: *composite materials; fibre/matrix interface; fibre debonding; pull-out tests; stress–displacement relation; two-way debonding theory; short fibre composites*

There are two undesirable properties of brittle materials that greatly limit their applications in structural components. Since brittle materials usually fail by the sudden unstable propagation of pre-existing cracks, no warning is provided before failure occurs. Moreover, the size of pre-existing cracks (which may form during processing, handling or service) is difficult to control and usually varies significantly from one component to another. As a result, the strength of components made with the same brittle material under similar processes can be very different. Brittle materials are thus also materials of low reliability.

The introduction of fibres into a brittle matrix can greatly improve its properties. The first-cracking strength (i.e., the applied tensile stress at which a crack is formed across a complete section of the material) of the composite can be increased significantly above that of the matrix itself.[1,2] The presence of fibres also greatly reduces the sensitivity of first-cracking strength to pre-existing flaw size.[3–5] Reliability is therefore highly improved. After first-cracking, provided the fibres are strong enough, the material can take further load (by the fibres themselves) until ultimate failure occurs (Fig. 1). With increased loading beyond the first-cracking strength, multiple cracks will be formed, giving rise to pseudo-ductility of the material.[1,6] This pseudo-ductility provides warning before final failure and also allows for stress redistribution to less severely loaded parts.

The desirable properties of composites described above are usually attainable in composite systems with sufficiently weak interfaces. In such systems, when a growing crack meets a fibre, debonding at the interface will occur. After the crack tip moves past the debonded fibres, bridging stress due to extension of the debonded fibres tends to close the crack and reduce the stress intensity at the crack tip (Fig. 2). Composite behaviour is then governed by the bridging stress *vs* crack opening relation for the fibres. As discussed by Marshall *et al.*[4] and Majumdar *et al.*,[7] the bridging stress *vs* half-crack

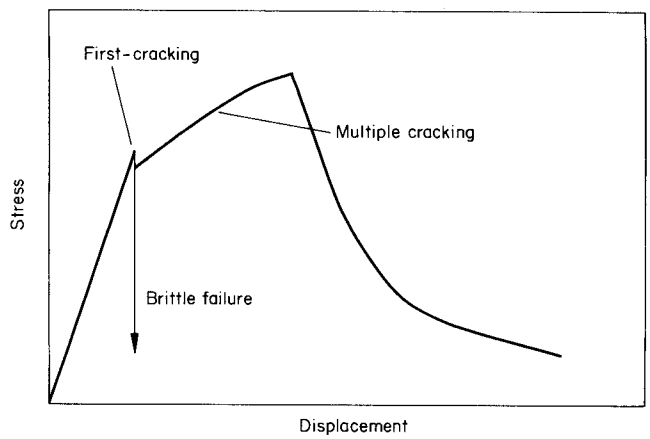

Fig. 1 Pseudo-ductility due to multiple cracking in fibre composites

0010-4361/90/070305-13

opening (p–u) relation is associated with the stress vs displacement (displacement of loaded fibre end relative to matrix surface) relation (σ_p–u relation) for a fibre pulled from the matrix through $p = V_f\sigma_p$, where V_f is the volume fraction of fibre. Hence, in order to predict composite behaviour, a model for the debonding of fibres pulled from the matrix is required. The debonding of continuous fibres has already been considered by Budiansky *et al.*[8] In this paper, we will concentrate on the debonding of fibres in short-fibre composites. In practice, both continuous and short fibres have been widely used in the reinforcement of brittle materials. Continuous fibre composites usually possess higher strength and modulus, while short-fibre composites offer the advantage of easy processing. In applications where a simple process is required to produce large volume of composite (e.g., fibre-reinforced concrete) or where components are of complex shapes (e.g., engine parts made of whisker-reinforced ceramics), short fibres are usually employed.

Theories for the debonding of discontinuous fibres have been developed by Greszczuk,[9] Takaku and Arridge,[10] Lawrence[11] and Gopalaratnam and Shah.[12] These are all one-way debonding theories, which consider debonding only from the loaded end of the fibre and neglect the possibility of fibre debonding from the embedded end. Such theories are only applicable to composites with low fibre volume fraction, low fibre/matrix moduli ratio and high interfacial strength/interfacial friction ratio. A two-way debonding theory, which is applicable to all general cases, has recently been developed by Leung and Li.[13] In the following sections, major findings from the new two-way theory are first summarized. The difference between composite behaviours, predicted by one-way and two-way debonding theories will be considered. For the fibre pull-out specimen, where fibre volume fraction is very low, a new method to derive interfacial properties based on a one-way debonding theory will be presented. For practical composite systems, the implications of the new two-way debonding theory to composite analysis and design will be discussed.

MAJOR FINDINGS FROM THE TWO-WAY DEBONDING THEORY

In this section, major findings from the two-way debonding theory developed by Leung and Li[13] will be described. A thorough discussion of the limitations of existing one-way debonding theories and the details of derivation of expressions for the two-way debonding theory can be found in Reference 13.

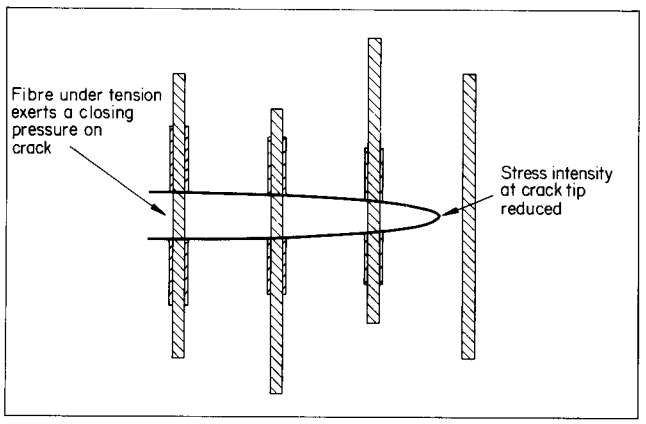

Fig. 2 Debonded fibres bridging a crack in the composite

Physical explanation for the two-way debonding phenomenon

Before findings of the two-way debonding theory are summarized, physical reasons for the two-way debonding phenomenon will be considered first. While it is well accepted that debonding can occur at the loaded end of the fibre, the possibility of debonding from the embedded end can be most easily explained by considering a very long fibre loaded at one end (Fig. 3). Stress transfer between fibre and matrix leads to continued decrease in fibre strain and increase in matrix strain. On continuing stress transfer along the interface, a point will eventually be reached where the longitudinal displacement in the matrix is higher than that in the fibre, which is physically impossible (Fig. 3(a)). What really happens is shown in Figs 3(b) and 3(c). When the fibre and matrix reach the same strain, the transfer of stress from one to the other is essentially terminated. The rest of the composite is under an applied constant strain (Fig. 3(c)). In a continuous fibre system, this constant strain will be sustained until the surface of the specimen is approached. In a discontinuous fibre composite with very little bond or anchorage at its embedded end, the stress at that end is zero. Hence, stress has to be transferred back into the fibre from the matrix. If the applied strain in Fig. 3(c) is high enough, debonding at the embedded end will take place. Two additional points should be noted.

1) There is negligible stress transfer between fibre and matrix when they reach the same strain only if the fibre is very long, so the stress conditions at the two ends of the fibre can essentially be uncoupled and considered separately as in Figs 3(b) and 3(c). For

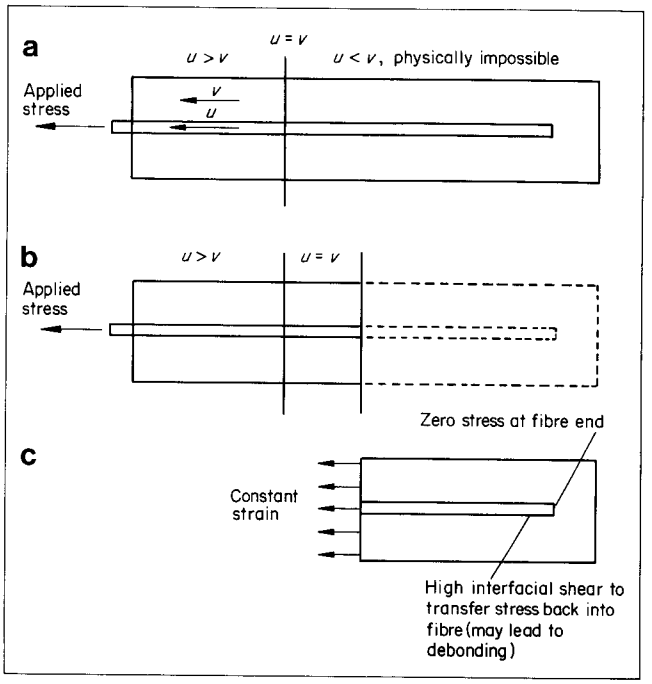

Fig. 3 Illustration of the physical reason for two-way debonding to occur

shorter fibres, the interfacial shear stress will simply reach a minimum when the fibre and matrix attain the same strain. The shear stress rises again towards the embedded end as stress is transferred from the matrix back to the fibre.

2) In the above discussion, the transfer of stress from fibre to matrix (Fig. 3(a)) can be elastic or frictional. Therefore, debonding from the embedded end can start either before or after the loaded end debonds.

When the applied load on an embedded fibre is increased, the scenerio is as shown in Fig. 4. When the applied load is low, debonding has not yet occurred and the stress distribution is elastic. This is referred to as the elastic stage (Fig. 4(a)). Further load increment leads to debonding from either the loaded end (Fig. 4(b)) or the embedded end (Fig. 4(c)), depending on the volume fraction and fibre/matrix moduli ratio. This is the one-way debonding stage. Continued debonding from one end of the fibre is accompanied by the increase of shear stress at the other end. When the shear stress at the other end also reaches the interfacial shear strength, two-way debonding will start to occur (Fig. 4(d)). Stress distributions for the various cases are given in the following. The derivation of the σ_p–u curve will also be described. Some useful expressions (obtained from the two-way debonding theory) for the derivation of σ_p–u relations are included in Appendix I.

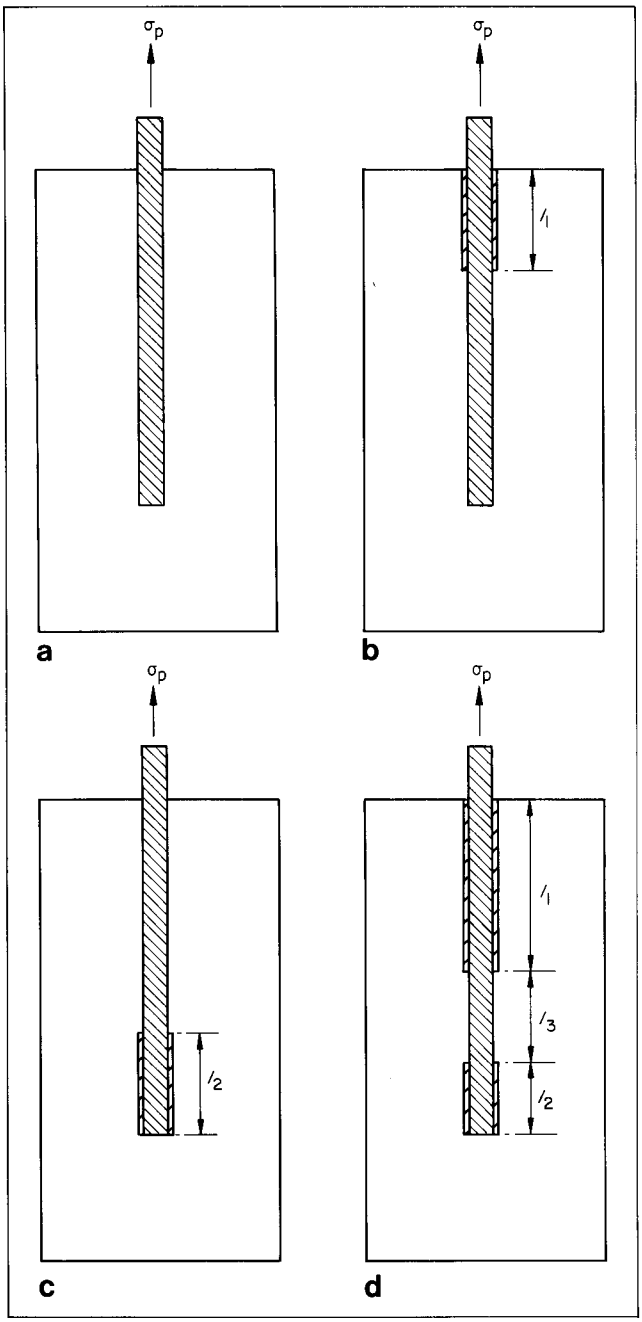

Fig. 4 Three different cases considered in the analysis: (a) elastic stage; (b) debonding from the loaded fibre end; (c) debonding from the embedded fibre end; and (d) debonding from both fibre ends

Elastic stage

$$\sigma f = A_1 - B_1 \sinh(\rho z/r_f) + C_1 \cosh(\rho z/r_f) \quad (1)$$

$$\tau_f = (\rho/2)\, B_1 \cosh(\rho z/r_f) - (\rho/2)\, C_1 \sinh(\rho z/r_f) \quad (2)$$

where

z = distance from the loaded end of the fibre

$A_1 = \alpha\sigma_p$

$B_1 = \sigma_p [(1-\alpha) \cosh(\rho L/r_f) + \alpha]/\sinh(\rho L/r_f)$

$C_1 = \sigma_p(1-\alpha)$

$\rho^2 = 2G_m E_c/[V_m E_m E_f \log(R^*/r_f)]$

$\log(R^*/r_f) = -[2\log V_f + V_m(3 - V_f)]/(4\, V_m^2)$

$\alpha = V_f E_f/E_c$

$E_c = V_f E_f + V_m E_m$

with E_m and E_f being the Young's moduli of matrix and fibre, G_m being the matrix shear modulus and V_f and V_m being the volume fractions of fibre and matrix, respectively. Also, L is the total fibre length and r_f is the fibre radius.

To determine which fibre end debonding will occur at first, we can look at the shear stresses (Equation (2)) at $z=0$ and $z=L$ respectively. From Equation (2), putting $z=0$ and $z=L$ respectively, we have

$$\tau_f(0) = (\rho/2)\sigma_p [\,(1-\alpha)\coth(\rho L/r_f) + \alpha/\sinh(\rho L/r_f)] \quad (3)$$

$$\tau_f(L) = (\rho/2)\sigma_p [\,\alpha\coth(\rho L/r_f) + (1-\alpha)/\sinh(\rho L/r_f)\,] \quad (4)$$

By comparing Equations (3) and (4), it can be shown that if α is less than 0.5, $\tau_f(0)$ will be greater than $\tau_f(L)$. Then, debonding will start at the loaded end. If α is greater than 0.5, $\tau_f(L)$ will be greater than $\tau_f(0)$ and debonding will start at the embedded end. These two cases are considered separately in the following.

One-way debonding stage

1. *$\alpha<0.5$ (debonding starts from the loaded end)*

Let l_1 be the length of the debonded zone (Fig. 4(b)).

For $z<l_1$:

$$\tau_f = \tau_i$$

$$\sigma_f = \sigma_p - 2\tau_i (z/r_f) \quad (5)$$

For $l_1 < z < L$:

$$\sigma_f = A_2 - B_2\sinh[\rho(z-l_1)/r_f] + C_2\cosh[\rho(z-l_1)/r_f] \quad (6)$$

$$\tau_f = (\rho/2)B_2\cosh[\rho(z-l_1)/r_f] - (\rho/2)C_2\sinh[\rho(z-l_1)/r_f] \quad (7)$$

where $A_2(\alpha,\sigma_p)$, $B_2(\tau_s,\rho)$ and $C_2(\tau_s,\rho,L,l_1,r_f,\alpha,\sigma_p)$ are given in Equation (27) of Appendix I.

From Equations (5) and (6), σ_p may be expressed in terms of l_1 (Equation (28) in Appendix I) by requiring the continuity of axial stress at $z = l_1$.

2. $\alpha > 0.5$ (debonding starts from the embedded end)

Let l_2 be the length of the debonded zone (Fig. 4(c)).

For $z > l_2$:

$$\tau_f = \tau_i \quad (8)$$

$$\sigma_f = 2\tau_i(L-z)/r_f$$

For $z < (L-l_2)$:

$$\sigma_f = A_3 - B_3\sinh[\rho z/r_f] + C_3\cosh[\rho z/r_f] \quad (9)$$

$$\tau_f = (\rho/2)\,B_3\cosh[\rho z/r_f] - (\rho/2)\,C_3\sinh[\rho z/r_f] \quad (10)$$

where $A_3(\alpha,\sigma_p)$, $B_3(\tau_s,\rho,L,l_2,r_f,\alpha,\sigma_p)$ and $C_3(\alpha,\sigma_p)$ are given in Equation (29) of Appendix I.

From Equations (9) and (10), σ_p may be expressed in terms of l_2 (Equation (30) in Appendix I) by requiring the continuity of axial stress at $z = L_2$.

Two-way debonding stage

After debonding is initiated at one of the fibre ends, further debonding is accompanied by continued increase of shear stress at the other fibre end. Eventually, when the shear stress at the other end also reaches the interfacial shear strength, the situation is as shown in Fig. 4(d).

In the debonded region near the loaded end ($0 < z < l_1$), the fibre and interfacial stresses are given by Equation (5). In the debonded region near the embedded end ($L-l_2 < z < L$), the stresses are given by Equation (8).

In the undebonded region, $l_1 < z < L-l_2$:

$$\tau_f = [\tau_s/(1+e^{-\rho l_3/r_f})]\,[e^{-\rho(z-l_1)/r_f} + e^{-\rho(l_1+l_3-z)/r_f}] \quad (11)$$

$$\sigma_f = \sigma_p - 2\tau_i(l_1/r_f) - (2/\rho)\,[\tau_s/(1+e^{-\rho l_3/r_f})]\,[1 - e^{-\rho(z-l_1)/r_f} + e^{-\rho(l_1+l_3-z)/r_f} - e^{-\rho l_3/r_f}] \quad (12)$$

where $l_3 = L-l_1-l_2$ is the length of the remaining undebonded zone.

l_1 and l_2 can be expressed in terms of σ_p and l_3 (Equations (31) and (32)). An expression between σ_p and the total debonded length l_1+l_2 can also be derived (Equation (33)).

It should be noted that, if $\alpha = 0.5$, debonding will start simultaneously at both ends and the analysis for two-way debonding in this sub-section holds once debonding occurs. Otherwise, two-way debonding will always be preceded by debonding from one end of the fibre.

Derivation of fibre stress–displacement (σ_p–u) relation

It should be noted that u is not sensitive to debonding at the embedded end of the fibre. Before the fibre debonds at its loaded end, the relative displacement can be obtained from:

$$u = |u_f - u_{R^*}| = \tau_f(0)\,[r_f\log(R^*/r_f)]/G_m \quad (13)$$

After debonding starts at the loaded end, u can be computed from the length of debonded zone l_1:

$$u/r_f = \tau_s\log(R^*/r_f)/G_m + (\sigma_p/E_f)\,(l_1/r_f) - \tau_i E_c\,(l_1/r_f)^2 / (E_f V_m E_m) \quad (14)$$

To obtain the σ_p–u relation, it is convenient to use the length of debonded zone as an intermediate parameter. The procedure for the computation of the σ_p–u relation is shown in the form of a flow chart in Fig. 5. For each point on the σ_p–u curve, a total debonded length l_d is first assumed. Then, depending on whether α is greater or less than 0.5, one-way debonding is assumed to be taking place with l_d being the length of debonded zone from one or the other end. A temporary stress σ_{pt} is first computed. The shear stress at the undebonded end is then checked to see if τ_s is reached. If τ_s has not been exceeded, the assumption of one-way debonding is correct and σ_p is equal to σ_{pt}. u can then be computed using the expressions for one-way debonding with l_1 or l_2 equal to l_d. On the other hand, if τ_s is exceeded on the other end as well, two-way debonding is taking place. Then, σ_p is computed from $l_d(=l_1+l_2)$ with the expression for two-way debonding. l_1 is then obtained from σ_p and u can be computed once l_1 is known.

σ_p–u relations predicted from one-way and two-way debonding theories

The derivation of σ_p–u relations with the two-way debonding theory has been described above. In the traditional one-way debonding theories, it is assumed that debonding always occurs at the loaded end of the fibre. The traditional one-way debonding theory can then be considered a simplified version of the above two-way debonding theory in which l_2 is always zero and Equation (28) in Appendix I is always used to compute σ_p from the debonded zone length.

σ_p–u relations obtained with one-way and two-way debonding theories for various values of fibre length, α and τ_s/τ_i have been compared in Reference 13. Two major conclusions can be made.

1) In general, if two-way debonding initiates before or at the point of maximum stress on the σ_p–u curve, two-way debonding theory has to be employed. For cases with short fibre length, low α and high τ_s/τ_i, maximum stress occurs before two-way debonding initiates and traditional one-way debonding approaches are appropriate. The transition value L^{tr}/r_f beyond which two-way debonding has to be considered is given by:

$$\rho L^{tr}/r_f = \cosh^{-1}(\tau_s/\tau_i) + [(1-2\alpha)/\alpha]\,[(\tau_s/\tau_i - 1)\,(\tau_s/\tau_i)] / [(\tau_s/\tau_i)^2 - 1]^{1/2} \quad (15)$$

for $\alpha < 0.5$; and

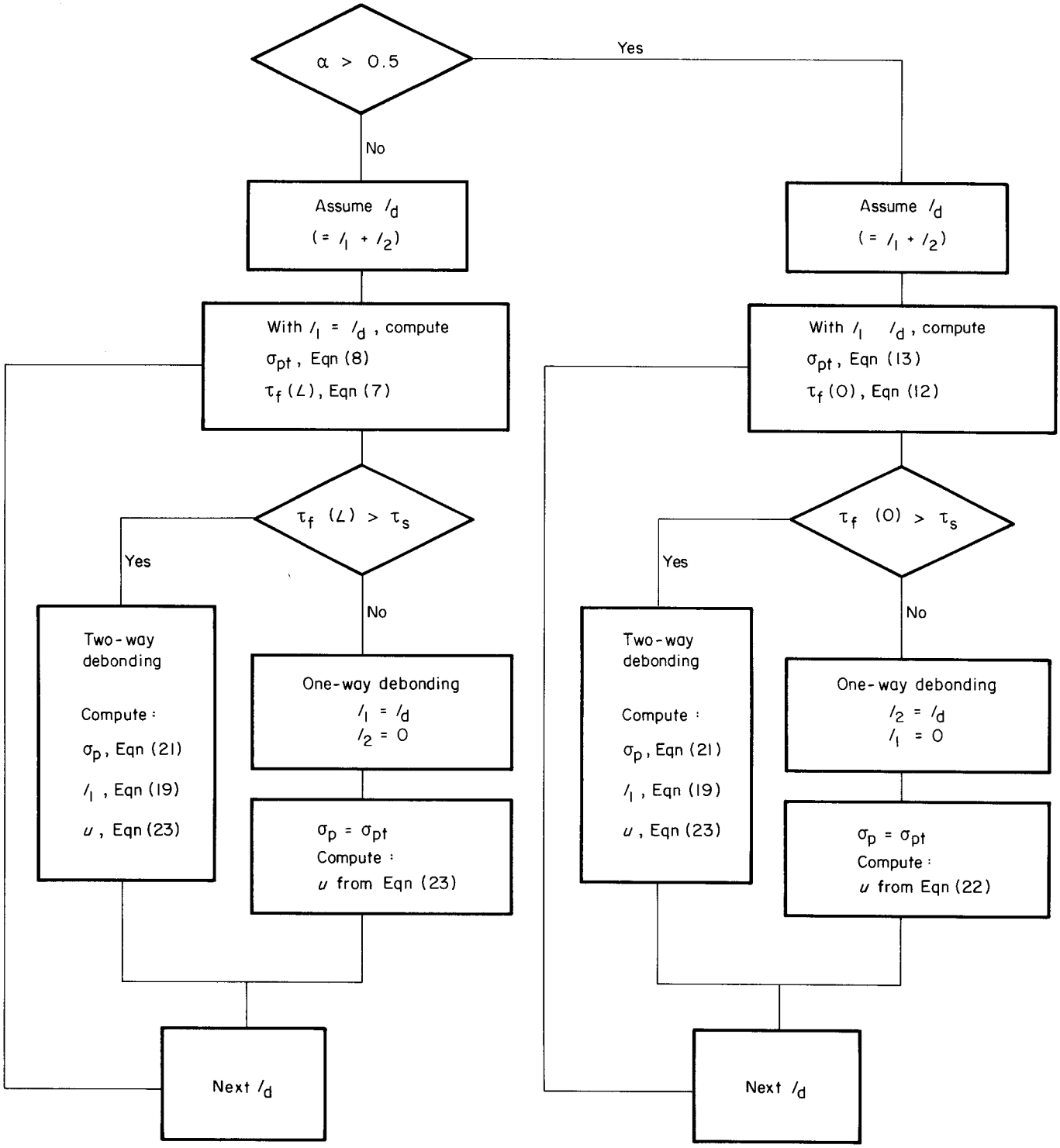

Fig. 5 Flow chart for the computation of σ_p–u relation with two-way debonding theory

$$\rho L^{tr}/r_f = \cosh^{-1}(\tau_s/\tau_i) + [(2\alpha-1)/(1-\alpha)] [(\tau_s/\tau_i - 1)(\tau_s/\tau_i)]/[(\tau_s/\tau_i)^2 - 1]^{1/2} \quad (16)$$

for $\alpha > 0.5$.

$\rho L^{tr}/r_f$ is plotted as a function of τ_s/τ_i for various values of α in Fig. 6. For $\alpha = x$ and $\alpha = 1-x$, the same line results. For each α, two-way debonding has to be considered if a point lies in the region to the left of the transition line. For $\alpha > 0.5$, debonding starts from the embedded end of the fibre and traditional one-way debonding theories (in which debonding always occurs from the loaded end) are never applicable. In general, the two-way debonding theory has to be employed. For very large α, however, a new one-way debonding theory, derived as a simplified form of the general two-way debonding theory to consider only debonding from the embedded end, may be used.

2) σ_p–u relations obtained from the one-way debonding theory always give a higher maximum stress. This is as expected because the neglecting of debonding from the embedded end leads to an overestimation of the stress carried by the

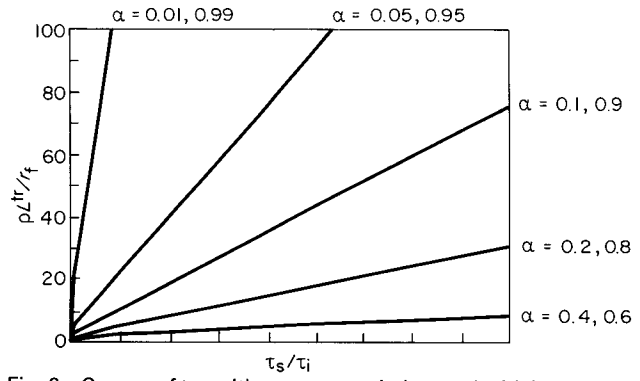

Fig. 6 Curves of transition aspect ratio beyond which two-way debonding theories have to be employed

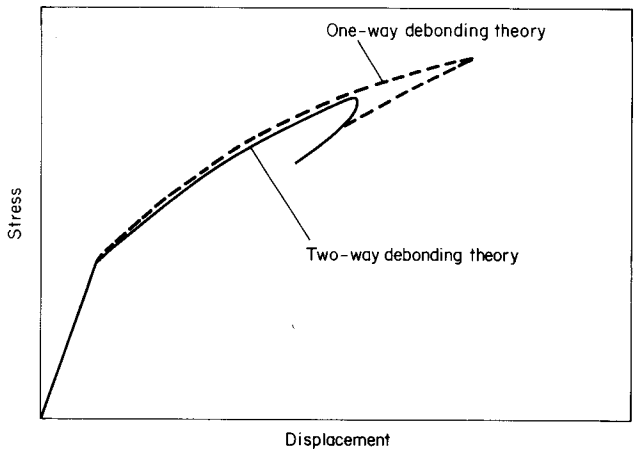

Fig. 7 σ_p–u relations predicted by one-way and two-way debonding theories

undebonded part of the interface. However, predictions from the two theories are usually very close to each other before the maximum stress obtained from the two-way debonding theory is reached (Fig. 7). The use of one-way debonding theory will therefore erroneously 'extend' the σ_p–u relations to a higher maximum stress. The implications of this result on macroscopic behaviour will be discussed in the following section.

MACROSCOPIC BEHAVIOUR PREDICTED FROM ONE-WAY AND TWO-WAY DEBONDING THEORIES

In this section, the relation between first-cracking strength and the σ_p–u relation will be discussed with a fracture mechanics approach. The problems with traditional one-way debonding theories in the prediction of first-cracking as well as post-first-cracking behaviour of composites will be considered.

A fracture mechanics approach has been used by Marshall *et al*[4,6] and Leung and Li[5] to study first-cracking behaviour of composites. In this approach, the propagation of a crack bridged by fibres embedded in an infinite matrix is considered. The stress intensity K_I at the crack tip is given by:

$$K_I = K_{appl} + K_{bridg} \tag{17}$$

where K_{appl} is the stress intensity due to the applied load and K_{bridg} is the stress intensity due to the bridging stresses in the fibre.

If a penny-shaped crack is assumed:

$$K_{appl} = 2\,(c/\pi)^{1/2}\sigma \tag{18}$$

$$K_{bridg} = 2\,(c/\pi)^{1/2}\int_0^1 p[u(X)]\,X\,dX/\sqrt{(1-X^2)} \tag{19}$$

where σ is the applied stress, c is the size of the pre-existing crack and $p[U(X)]$ is the fibre bridging stress as a function of half-crack opening displacement along the crack profile.

When K_I reaches a critical value K_{IC}, the crack will propagate unstably across the whole section of the material. The applied stress σ_{fc} at this moment is then by definition the first-cracking strength of the composite.

From Equations (17)–(19), σ_{fc} is given by:

$$\sigma_{fc} = 0.5\,(\pi/c)^{1/2}K_{IC} + \int_0^1 p[u(X)]\,X\,dX/\sqrt{(1-X^2)} \tag{20}$$

The second term in the right-hand side of Equation (20) shows the contribution of bridging fibres to the first-cracking stress. The p vs. u relation is associated with the σ_p–u relation described in the above section through $p=V_f\sigma_p$. In Fig. 7, only the σ_p–u relation during debonding is given. After debonding is completed, the fibre will be pulled out against the friction at the interface. If constant friction is assumed during the pull-out process, the pull-out branch of the σ_p–u relation will be a straight line with $\sigma_p=0$ at u=half of the fibre length corresponding to the maximum embedded length. It can be observed from Fig. 7 that debonding becomes unstable soon after the maximum stress is reached. In practice, the unstable branch cannot be obtained. Once instability commences, the stress simply drops to a point corresponding to the same value of u on the pull-out branch (Fig. 8(a)). Since the instability point and the point of maximum stress are very close, they are taken to be the same point. Because the fibre length is much larger than the value of u at maximum stress, the pull-out branch is very flat compared with the debonding branch of the σ_p–u curve. Hence, one can assume that while one-way and two-way debonding theories predict different maximum stresses, the pull-out branch of their σ_p–u relation is the same (Fig. 8(a)).

To obtain the p–u relation for the composite, one has to know the distribution of fibres in the composite. If a uniform distribution of aligned fibres is assumed, the composite p–u relation is approximately of the form shown in Fig. 8(b). The calculation of actual p–u relations involves the computation of average stress carried at each u for fibres of different embedded lengths. For the purpose of discussion here, it suffices to know the qualitative difference between p–u curves predicted by one-way and two-way debonding theories. Similar to the case of a single fibre, one-way debonding theory overestimates the stress at a certain range of u. The distribution of bridging stresses along the crack profile predicted by the two debonding theories is shown qualitatively in Fig. 8(c) with the assumption that the difference in p–u relations shown in Fig. 8(b) will not give rise to significantly different crack profiles. It is suggested in Fig. 8(c) that the contribution of bridging fibres to resist crack propagation (i.e., the

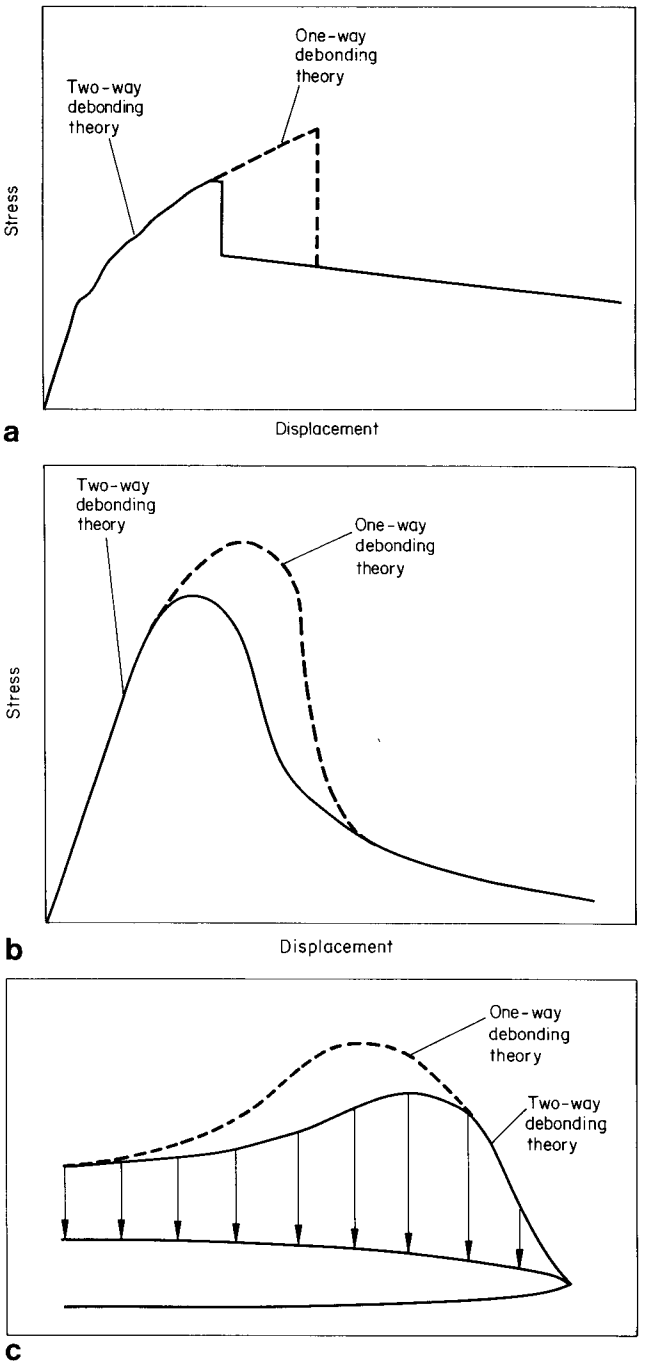

Fig. 8 (a) p–u relation for a single fibre; (b) p–u relation for all fibres; and (c) distribution of bridging stress along the crack, predicted by one-way and two-way debonding theories

integral in Equation (20)) and hence the first-cracking strength of the composite are overestimated if one-way debonding theory is employed.

Besides the overestimation of first-cracking stress, the use of one-way debonding theory can also overestimate the reliability of composites and indicate erroneously the presence of multiple cracking. As discussed by Marshall *et al.*[4] and Leung and Li,[5] when the crack opens due to applied load, if the bridging stress in the most heavily loaded fibres (i.e., the fibres furthest away from the crack tip) becomes equal to the applied stress, the increase in K_{appl} with further increase in crack size is exactly balanced by the increase in K_{bridg}

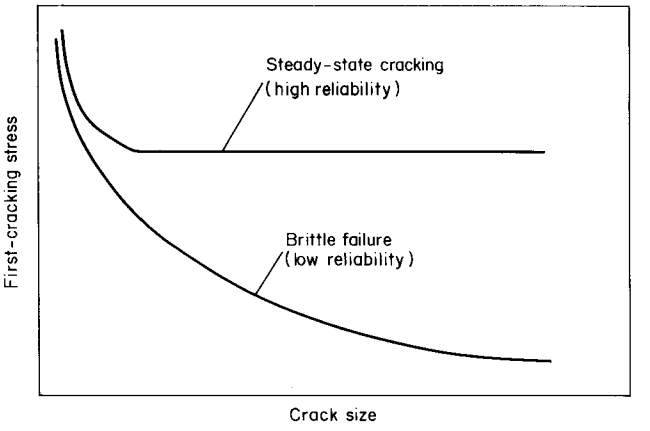

Fig. 9 Steady-state cracking with uniform first-cracking strength for a range of crack sizes

associated with the enlargement of the bridging zone. At this steady-state cracking, the crack propagates under constant stress (Fig. 9). If the inherent flaw size of a material happens to lie close to the range of constant stress, the first-cracking strength will be almost independent of flaw size, thus implying a very high reliability. Moreover, if the first-cracking stress is lower than the maximum stress on the p–u curve, the composite can take further load (by the fibres alone) before ultimate strength is reached. Multiple cracking will then occur, giving rise to pseudo-ductility. Steady-state cracking and multiple cracking are clearly more likely to occur if the maximum stress on the p–u curve is increased (while keeping the shape of the curve unchanged). Therefore, the overestimation of maximum p due to the use of one-way debonding theories may lead to the erroneous impression that a certain composite is highly reliable and will give warning before ultimate failure. Assumptions of such desirable behaviours, as well as an overestimated strength, may lead to non-conservative designs and unexpected sudden failure of structural components. Unrestrained applications of traditional one-way debonding theories can lead to unsafe designs and should therefore be avoided. For general applications, the two-way debonding theory should be employed.

INTERPRETATION OF FIBRE PULL-OUT TEST RESULTS

Before composite behaviour can be predicted, the two interfacial parameters, τ_s and τ_i, have to be obtained. The fibre pull-out test is a very common test to determine fibre/matrix interfacial properties. In Gopalaratnam and Shah,[12] τ_s and τ_i were obtained by trial and error to determine the combination of τ_s and τ_i that would give load–displacement curves closest to experimental pull-out test results. In Bartos,[14] a method which involved graphical fitting was used to determine τ_s and τ_i from the pull-out test results. Such techniques involve a lot of subjective judgement and are relatively time consuming. In this section, we will describe a simple technique for the deduction of τ_s and τ_i from fibre pull-out test results.

A typical result from a fibre pull-out test is shown in Fig. 10. The load vs. displacement curve shown in the

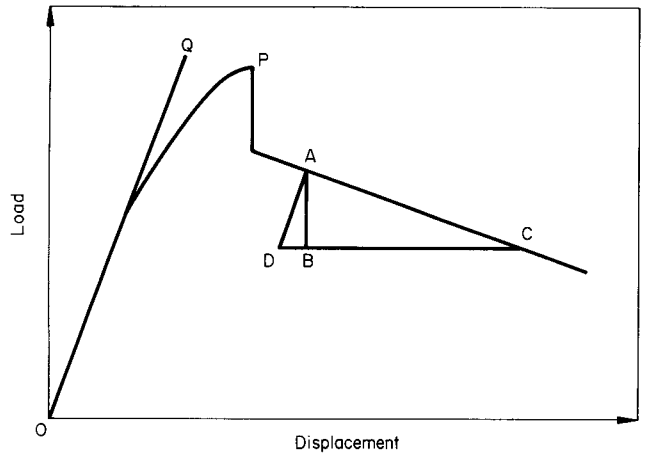

Fig. 10 Pull-out test result with linear pull-out branch

figure shows a straight pull-out branch. This is consistent with the debonding theory described above and is for the idealized case where there is no Poisson's effect or slip strengthening or weakening at the interface (Wang *et al*;[15] Li *et al*[16]). Means to extend our theory to those other cases will be discussed later in this section. The determination of τ_i from the pull-out curve is relatively straightforward. The slope of the pull-out branch is equal to $-(2\pi r_f \tau_i)$. However, the slope from the test results cannot be used directly because unloading of the loading fixture and the free (unembedded) part of the fibre have to be considered. Correction for unloading is very important because a flexible chain of loading fixture is usually employed in a pull-out test to ensure good alignment and deformation of this flexible chain cannot be neglected. A simple way of correction is shown in Fig. 10. The unloading is assumed to follow the initial slope of the loading part of the curve. Hence, for a load drop from point A to point C, the fibre slips by a distance not equal to BC but equal to DC, where AD is parallel to the initial loading slope OQ. τ_i is then equal to $(AB/DC)/2\pi r_f$.

After τ_i is determined, τ_s can be obtained from the peak load. One important point to be noticed is that the volume fraction of fibre in a pull-out test is usually very small, estimated to be about 10^{-6} to 10^{-4}. As a result, α is very small and for reasonable fibre embedded lengths (usually less than $100r_f$ but greater than about $20r_f$), the use of one-way debonding theory (with debonding starting from the loaded end) is a good approximation. To obtain τ_s, one recalls that the applied stress in terms of debonded length l_1 is given by Equation (28) in Appendix I as follows:

$$\sigma_p = [2(l_1/r_f)\tau_i \cosh X_1 + 2(\tau_s/\rho)\sinh X_1] / [(1-\alpha)\cosh X_1 + \alpha]$$

where $X_1 = \rho(L - l_1)/r_f$.

The maximum stress can then be obtained by differentiating Equation (28) and setting the result to zero. For $\alpha << 1$, the debonding zone length l_1 at maximum stress is given by:

$$\cosh[\rho(L-l_1)/r_f] = \sqrt{(\tau_s/\tau_i)} \quad (21)$$

Substituting into Equation (28), again taking $\alpha = 0$, the peak stress, σ_{peak}, is given by:

$$\sigma_{peak}/[2(L/r_f)\tau_i] = 1 + \{\sqrt{[(\tau_s/\tau_i)^2 - (\tau_s/\tau_i)]} - \cosh^{-1}\sqrt{(\tau_s/\tau_i)}\}/(\rho L/r_f) = P_{peak}/(2\pi r_f L \tau_i) \quad (22)$$

where P_{peak} is the peak load on the pull-out load–displacement curve.

For the pull-out specimen, L/r_f is the embedded fibre length. ρ cannot usually be determined precisely because the pull-out specimen is normally not of cylindrical shape and, strictly speaking, our theory does not hold. An approximation of ρ can be obtained by assuming that the fibre is surrounded by a cylindrical volume of matrix with the same volume of matrix material as in the pull-out specimen. Then, as before, ρ can be deduced from V_f, E_f, E_m and G_m.

Also, our debonding theory is developed for the boundary condition of zero stress at the free matrix surface and is applicable to the pull-out specimen shown in Fig. 11(a). However, specimens with load applied onto the matrix surface (Fig. 11(b)) are also very common. The difference between the stress distribution in these two cases can be obtained by solving the problem with the boundary conditions shown in Fig. 11(c). This is done in Appendix II and the result is:

$$\sigma_f = \alpha\sigma_p \{1 - \cosh(\rho z/r_f) - [1 - \cosh(\rho L/r_f)]\sinh(\rho z/r_f)/\sinh(\rho L/r_f)\} \quad (23)$$

$$\tau_f = (\rho/2)\alpha\sigma_p \{\sinh(\rho z/r_f) + [1 - \cosh(\rho L/r_f)]\cosh(\rho z/r_f)/\sinh(\rho L/r_f)\} \quad (24)$$

For the pull-out specimen, α is very small. As a result, the axial and shear stresses given by Equations (23) and (24) are both very small. The difference in stress distributions between the pulled-out specimens shown in Fig. 11(a) and 11(b) are therefore negligible.

For practical brittle matrix systems (such as synthetic fibre- or steel fibre-reinforced concrete, glass fibre-reinforced resin and carbon fibre-reinforced glass), ρ ranges from about 0.075 to 1.1. Since the embedded length usually varies from about $20r_f$ to $100r_f$, the value of $\rho L/r_f$ varies from 1.5 to 110. In Fig. 12, $P_{peak}/(2\pi r_f L\tau_i)$ is plotted against (τ_s/τ_i) for various values of $\rho L/r_f$. Once τ_i is known, one can compute $P_{peak}/(2\pi r_f L\tau_i)$. After computing $\rho L/r_f$ for the particular specimen, τ_s can be obtained from Fig. 12 (or by numerically solving Equation (22)). Of course, Fig. 12 is shown here for the purpose of illustration. To obtain the best results, a curve corresponding to the specific value of $\rho L/r_f$ for the pull-out specimen employed should be plotted with Equation (22).

In the above, only the case with a linear pull-out branch has been considered. In some cases, the pull-out branch can either concave upwards (Fig. 13(a)) or downwards (Fig. 13(b)). These two types of pull-out behaviour are due to different reasons and will be discussed in the following. (Note: results showing increasing stress with pull-out have been reported by Wang *et al.*[15] In such cases, abrasion between fibre and matrix leads to a significant increase in interfacial friction. Then, τ_s and

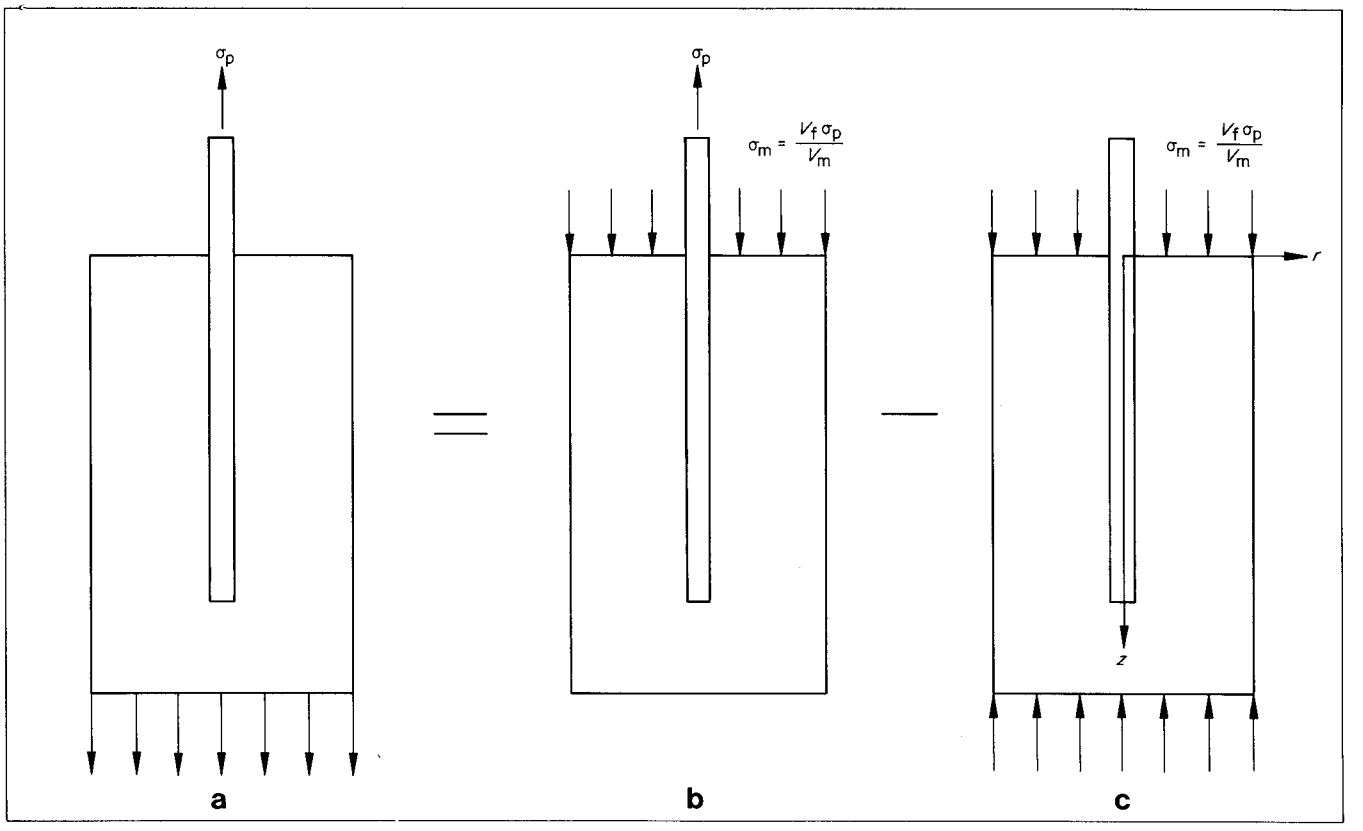

Fig. 11 (a) and (b) Two different types of pull-out specimen configuration; and (c) model to compute the difference in stress distribution for the two specimens in (a) and (b)

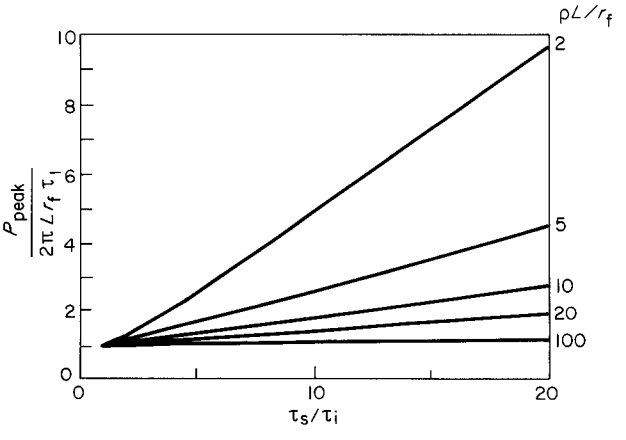

Fig. 12 Theoretical curves for the determination of interfacial strength/friction ratio from fibre pull-out test results

the initial τ_i are no longer important parameters. A stress increment *vs* fibre slip relation is more appropriate to characterize the interface.)

Pull-out test results with a shape shown by Fig. 13(a) (concaving upwards) have been obtained by Naaman and Shah.[17] This kind of behaviour can be explained by the fact that the matrix is being abraded by the fibre during pull-out. Abrasion leads to an increase in the size of the 'tunnel' containing the fibre. Hence, the resistance to further pull-out is decreased. Wang *et al*[15] have suggested the use of a stress–slip (τ–s) relation at the interface to model the decrease of interfacial resistance with increasing relative slip between the fibre and matrix. However, since the abrasion effect is significant only when relative slip between fibre and matrix is high, the effect can be neglected during the debonding stage. Therefore, once we identify the point

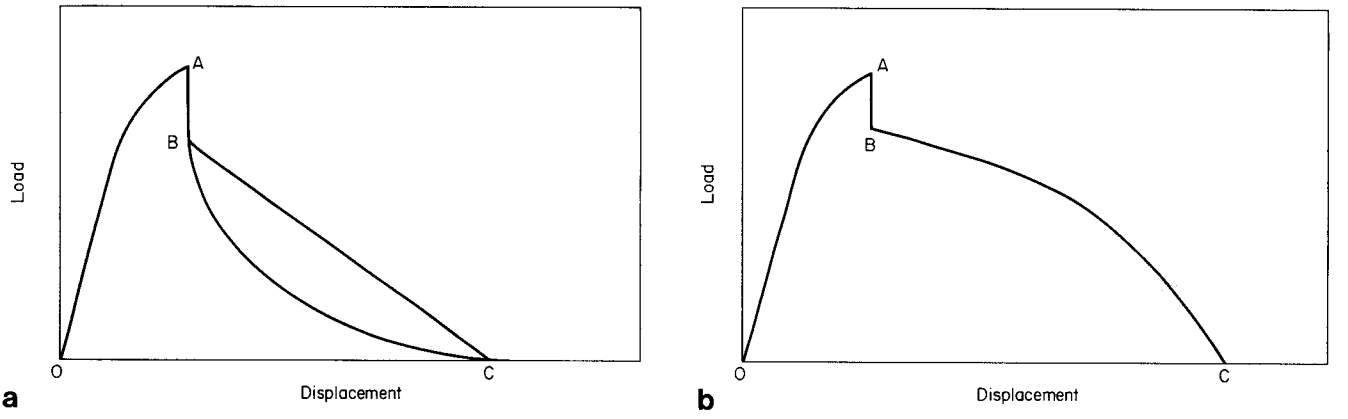

Fig. 13 Pull-out test data with non-linear pull-out branch

on the pull-out branch where the load drop is arrested (point B in Fig. 13(a)), the interfacial friction τ_i before abrasion damage can be obtained from the slope of a line joining point B and the point at which stress has decreased to zero. The interfacial strength τ_s can then be obtained from Fig. 12 as described above. In cases where significant abrasion leads to a steep drop of the pull-out curve, the determination of point B from the plotted data may not be easy. However, the drop of stress to point B is a sudden event and during the performing of pull-out experiments, one should note the stress just after the unstable drop and take this as the stress value at point B. It should also be noted that it is not correct to compute τ_i from the initial slope of the pull-out branch (i.e., slope of the data curve at point B) because this slope is dependent on τ_i as well as the initial slope of the τ–s curve.

Test results with a pull-out branch concaving downwards (Fig. 13(b)) have been obtained by Takaku and Arridge[10] for steel in epoxy resin. As explained by Takaku and Arridge, this shape is due to Poisson's effect on the interfacial compressive stress. When the fibre is pulled, it shrinks away from the matrix, leading to a reduction in interfacial compression and thus a reduction in the interfacial friction. The reduction of interfacial friction depends on the applied load which decreases when the fibre is pulled out. In other words, when the fibre is pulled out, the interfacial friction increases, thus leading to the observed shape of the pull-out curve. In Reference 10, a method is suggested to fit a curve to the data to obtain both the initial compressive stress σ_0 and the interfacial friction coefficient μ. In this case, debonding of the fibre and hence the peak load are both affected by Poisson's effect. For example, for $\alpha<0.5$, (Fig. 4(b)), in the debonded zone ($0<z<l_1$), the stress can be obtained by solving

$$d\sigma_f/dz = (2/r_f)\,\mu\,(\sigma_0 - k\sigma_f) \qquad (25)$$

with the boundary condition $\sigma_f=\sigma_p$ at $z=0$. The solution is given by:

$$\sigma_f = (1/k)\,[\sigma_0 - (\sigma_0 - k\sigma_p)\exp(2k\mu z/r_f)] \qquad (26)$$

where $k = E_m\upsilon_f/[E_f(1+\upsilon_m)]$ as shown in Reference 10 with υ_f and υ_m being the Poisson's ratios of the fibre and matrix.

The peak strength can then be obtained by first combining Equations (6) and (25) to obtain a relation between σ_p and l_1. By differentiation, the value of l_1 at maximum stress can be obtained. The maximum stress can then be expressed as a function of the other variables. The approach is very similar to the case with constant interfacial friction though the resulting expressions will be more complicated.

Poisson's effect decreases τ_i and increases τ_s/τ_i. As discussed in Reference 13 and shown by Piggott,[18] the validity of strength-based debonding theories (i.e., theories with the reaching of interfacial strength as the debonding criterion) is questionable for large τ_s/τ_i. However, at present, there are no better debonding theories available and the value of τ_s/τ_i marking the limit of validity for strength-based theories has not been determined. Therefore, it suffices to suggest that whenever Poisson's effect is significant, one should check the minimum value of τ_i that results. If τ_i is much smaller than τ_s, results should be interpreted with care.

IMPLICATIONS OF NEW THEORY TO PRACTICAL COMPOSITE SYSTEMS

The limits of applications for the one-way debonding theory have already been discussed above. In this section, several practical composite systems will be considered to see whether such limits are reached and hence whether two-way debonding theory has to be employed. Composite systems considered below include steel fibre-reinforced concrete, glass fibre-reinforced polyester resin and graphite fibre-reinforced borosilicate glass.

For steel fibre-reinforced concrete, Gopalaratnam and Shah[12] obtained values for τ_s and τ_i of 4.134 MPa (600 psi) and 1.895 MPa (275 psi) respectively. In their work, although the pull-out curve is concaving upwards, a constant τ_i was assumed. However, since curve fitting has been carried out for several fibre lengths and good agreement has been obtained between experimental and predicted peak load, their estimates for τ_s and τ_i are considered reasonable. For these values of τ_s and τ_i, τ_s/τ_i is about 2. Normally, the volume fraction of steel fibre used in concrete is from 0.5 to 2%, corresponding to values of α ranging from 0.034 to 0.125 and ρ from 0.243 to 0.314 (E_f=210 MPa, E_m=30 MPa and υ_m=0.3). The fibre aspect ratio $(L/r_f)^{tr}$ for the transition from one-way to two-way debonding for the two volume fractions are respectively 135.7 and 26.3. Common aspect ratios for steel fibre used in concrete range from about 40 to 100. (Note: this aspect ratio is usually defined as the ratio of fibre length to fibre diameter, which is the same as the ratio of maximum fibre embedded length to fibre radius.) Therefore, for V_f=0.5%, one-way debonding theory is appropriate. However, for V_f=2.0%, two-way debonding theory has to be employed.

Pull-out test results for glass fibre-reinforced polyester resin can be found in Chua and Piggott[19] and are shown in Fig. 14. Piggott[18] has shown that strength-based theories cannot explain the variation of maximum

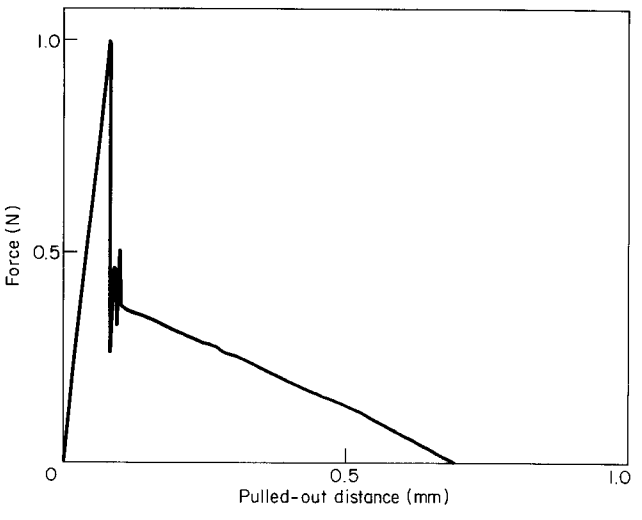

Fig. 14 Typical pull-out curve for glass fibre in polyester (from Reference 19)

pull-out load with embedded length. This is probably due to the Poisson's contraction that greatly reduces the interfacial friction at the onset of debonding. From Fig. 14, the pull-out branch of the experimental curve appears to be very straight, showing that Poisson's effect is not significant. However, since Poisson's contraction is directly proportional to the applied stress, while it may not be important at low applied stress (such as at the pull-out branch), it may be important during debonding. At the peak load of 1 N (Fig. 14), the fibre is under a stress of 2.63 GPa, giving a Poisson's contraction of about 0.75%. In the following, for discussion purposes, it is assumed that Poisson's effect can be neglected and strength-based theories can be used. For this material system, r_f=11 μm, E_f=70 GPa, E_m=2.5 GPa and υ_m=0.2. The size of specimen is not known exactly and will be assumed to be cylindrical with a radius of 5 mm, thus giving a volume fraction of 4.84×10^{-6}. The value of τ_s/τ_i for this system can then be obtained from the experimental data. From Fig. 14, $P_{peak}/(2\pi r L\tau_i)$=2.5. The embedded length of the fibre is 0.7 mm, giving a value of $\rho L/r_f$ equal to 4.74. τ_s/τ_i is then approximately equal to 10. For practical short fibre composites with glass fibre in polyester resin, the volume fraction of fibre ranges from about 15 to 30%. The corresponding values of α and ρ are from 0.832 to 0.923 and 0.61 to 1.21, respectively. Also, in practical composites, the glass fibres are in bundles which are bonded together and act as individual reinforcing members. The size of the bundle depends on the degree of dispersion and it is assumed here that each bundle consists of 400 fibres and thus has an effective radius of 20 × 0.011=0.22 mm. For V_f=15%, $(L/r_f)^{tr}$=63.5 while for V_f=30%, $(L/r_f)^{tr}$=84.6. The fibre length employed in short fibre composites is usually around 25.4 mm, giving a maximum embedded length of 12.7 mm and aspect ratio of 57.7. Hence, one-way debonding theory is sufficient to model the behaviour of the glass fibre/polyester composite system described above. However, since α>0.5 for all practical volume fractions, traditional one-way debonding theory cannot be used. A new one-way debonding theory for debonding from the embedded end has to be employed.

Graphite fibre-reinforced borosilicate glass has been processed and studied by Sambell *et al.*[20] Pull-out test results for this system are not available, probably due to the difficulties in specimen preparation as well as testing when the fibre is of such a small size (4 μm radius). However, it was reported in Reference 20 that graphite fibres pulled out from the failure surface of the borosilicate composite are relatively clean, with thin films of glass attaching to the fibre only in some cases. In contrast, in other systems such as graphite-reinforced magnesia, crystals of the matrix material are found adhering to the fibre. It is therefore evident that the bond between borosilicate and graphite is not very strong. τ_s/τ_i is thus expected to be low and is assumed to be in the range from 2 to 5. For this system, E_f=380 GPa, E_m=70 GPa, υ_m=0.3. V_f ranges from 10–30%. For V_f=10%, α=0.376 and ρ=0.607, giving $(L/r_f)^{tr}$ =3.42 and 8.21 for τ_s/τ_i=2 and 5, respectively. For V_f=30%, α=0.699 and ρ=1.3356, giving $(L/r_f)^{tr}$ =2.13 and 5.76 for τ_s/τ_i=2 and 5, respectively. In the composite, the mean fibre length is about 200 μm, that is, the mean aspect ratio is about 25. This is much higher than the value of $(L/r_f)^{tr}$ for all practical volume fractions and hence two-way debonding theory must be employed for this system.

CONCLUSIONS

Traditional one-way debonding theories are only applicable to composites with low volume fraction, low fibre length and/or high interfacial shear strength/friction ratio. The application of one-way debonding theories to more general cases leads to overestimation of strength and reliability of composites, thus leading to unconservative designs. With τ_s and τ_i determined from fibre pull-out test results, the significance of applying two-way debonding theory to the design and analysis of practical composite systems can be assessed.

REFERENCES

1 **Aveston, J., Cooper, G.A. and Kelly, A.** 'Single and multiple fracture', in *The Properties of Fiber Composites* (Conference Proceedings, National Physical Laboratory, IPC Science and Technology Press Ltd, UK, 1971) pp 15–24

2 **Hannant, D.J., Hughes, D.C. and Kelly, A.** 'Toughening of cement and other brittle solids with fibres' *Phil Trans Roy Soc London* **310** (1983) pp 175–190

3 **Kendall, K., Alford, N.McN. and Birchall, J.D.** 'Weibull modulus of toughened ceramics' in *Advanced Structural Ceramics* (Material Research Society Symposium Proceeding, **78** (1987) pp 189–197

4 **Marshall, D.B., Cox, B.N. and Evans, A.G.** 'The mechanics of matrix cracking in brittle-matrix fiber composites' *Acta Metallurgica* **33** No 11 (1985) pp 2013–2021

5 **Leung, C.K. and Li, V.C.** 'First-cracking strength of short-fiber reinforced ceramics' *Ceramic Eng and Sci Proc* **10** No 9–10 (1989) pp 1164–1178

6 **Marshall, D.B. and Cox, B.N.** 'Tensile fracture of brittle matrix composites: influence of fiber strength' *Acta Metallurgica* **35** No 11 (1987) pp 2607–2619

7 **Majumdar, B.S., Newaz, G.M. and Rosenfield, A.R.** 'Yielding behavior of ceramic matrix composites' *Proc Seventh Int Conf on Fracture* **4** (1989) pp 2805–2814

8 **Budiansky, B., Hutchinson, J.W. and Evans, A.G.** 'Matrix fracture in fiber-reinforced ceramics' *J Mech Phys Solids* **34** No 2 (1986) pp 167–189

9 **Greszczuk, L.B.** 'Theoretical studies of the mechanics of the fiber–matrix interface in composites' *ASTM STP 452* (American Society for Testing and Materials, Philadelphia, 1969) pp 42–58

10 **Takaku, A. and Arridge, R.G.C.** 'The effect of interfacial radial and shear stress on fiber pull-out in composite materials' *J Phys D: Appl Phys* **6** (1973) pp 2038–2047

11 **Lawrence, P.** 'Some theoretical considerations of fiber pull-out from an elastic matrix' *J Mater Sci* **7** (1972) pp 1–6

12 **Gopalaratnam, V.S. and Shah, S.P.** 'Tensile fracture of steel fiber reinforced concrete' *ASCE J Engng Mech* **113** No 5 (1987) pp 635–653

13 **Leung, C.K. and Li, V.C.** 'A new strength-based theory for the debonding of discontinuous fibers in an elastic matrix' submitted to *J Mater Sci* (1989)

14 **Bartos, P.** 'Analysis of pull-out tests on fibers embedded in brittle matrices' *J Mater Sci* **15** (1980) pp 3122–3128

15 **Wang, Y., Li, V.C. and Backer, S.** 'Modelling of fiber pull-out from a cement matrix' *Int J Cement Composites and Lightweight Concrete* **10** No 3 (1988) pp 143–149

16 **Li, V.C., Wang, Y. and Backer, S.** 'A statistical-micromechanical model of tension-softening behaviour of short fiber reinforced brittle matrix composites' submitted to *J Mech Phys Solids* (1989)

17 **Naaman, A.E. and Shah, S.P.** 'Pull-out mechanism in steel fiber reinforced concrete' *J Structural Div, ASCE* **102** No ST8 (1976) pp 1537–1548

18 **Piggott, M.R.** 'Debonding and friction at fiber–polymer interfaces. I: criteria for failure and sliding' *Composites Sci and Technol* **30** (1987) pp 295–306
19 **Chua, P.S. and Piggott, M.R.** 'The glass fiber–polymer interface: II—work of fracture and shear stresses' *Composites Sci and Technol* **22** (1985) pp 107–119
20 **Sambell, R.A.J., Bowen, D.H. and Phillips, D.C.** 'Carbon fiber composites with ceramic and glass matrices' *J Mater Sci* **7** (1972) pp 663–675

AUTHORS

Whilst both authors are with the Department of Civil Engineering, Massachusetts Institute of Technology, Cambridge, MA 02139, USA, V. C. Li is presently affiliated with the Advanced Civil Engineering Materials Research Laboratory at the University of Michigan, Department of Civil Engineering, Ann Arbor, MI, 48109-2125, USA. Enquiries should be directed to Professor Li in the first instance.

Appendix I

SOME USEFUL EXPRESSIONS DERIVED BY THE TWO-WAY DEBONDING THEORY

In this appendix, some expressions required for the derivation of σ_p–u relations are given. For the derivation of such expressions, one should refer to a companion paper[13] by the authors.

$\alpha<0.5$ (debonding starts from the loaded end, Fig. 4(a))

The constants A_2, B_2 and C_2 for fibre axial stress (Equation (6)) and interfacial shear stress (Equation (7)) are given by:

$$A_2 = \alpha\sigma_p$$
$$B_2 = 2\,(\tau_s/\rho) \tag{27}$$
$$C_2 = \{\, 2\,(\tau_s/\rho)\sinh\,[\rho(L-l_1)/r_f] - \alpha\sigma_p\,\} \Big/ \cosh[\rho(L-l_1)/r_f]$$

Using Equations (5) and (6) the continuity of stress at $z=l_1$ provides a relation between l_1 and σ_p.

$$\sigma_p = [\,2(l_1/r_f)\tau_i\cosh X_1 + 2(\tau_s/\rho)\sinh X_1] \Big/ [(1-\alpha)\cosh X_1 + \alpha] \tag{28}$$

where $X_1 = \rho(L-l_1)/r_f$.

$\alpha>0.5$ (debonding starts from the embedded end, Fig. 4(b))

The constants A_3, B_3 and C_3 for fibre stress (Equation (9)) and interfacial shear (Equation (10)) are given by:

$$A_3 = \alpha\sigma_p$$
$$B_3 = \{\, 2(\tau_s/\rho) + (1-\alpha)\sigma_p\sinh[\rho(L-l_2)/r_f]\,\} \Big/ \cosh[\rho(L-l_2)/r_f] \tag{29}$$
$$C_3 = (1-\alpha)\sigma_p$$

Using Equations (8) and (9) as well as the continuity of stress at $z=l_2$, σ_p can be expressed in terms of l_2 as:

$$\sigma_p = [\,2(l_2/r_f)\tau_i\cosh X_2 + 2(\tau_s/\rho)\sinh X_2] \Big/ [\alpha\cosh X_2 + (1-\alpha)] \tag{30}$$

where $X_2 = \rho(L-l_2)/r_f$.

Two-way debonding (Fig. 4(c))

Expressions for the fibre axial stress and interfacial shear stress are already given in the text (Equations (5), (8), (11) and (12)).

In Equations (11) and (12) (with $l_3=L-l_1-l_2$), l_1 and l_2 can be related to σ_p by:

$$2\tau_i(l_1/r_f) = (1-\alpha)\sigma_p - (2/\rho)\tau_s[1-e^{-\rho l_3/r_f}] \Big/ (1+e^{-\rho l_3/r_f}) \tag{31}$$

$$2\tau_i(l_2/r_f) = \alpha\sigma_p - (2/\rho)\tau_s[1-e^{-\rho l_3/r_f}]/(1+e^{-\rho l_3/r_f}) \tag{32}$$

By adding Equations (31) and (32) together, the applied stress σ_p can be expressed in terms of the total debonded zone length $(l_1 + l_2)$ as:

$$\sigma_p = 2\tau_i(l_1+l_2)/r_f + (4/\rho)\tau_s[1-e^{-\rho(L-l_1-l_2)/r_f}] \Big/ (1+e^{-\rho(L-l_1-l_2)/r_f}) \tag{33}$$

Appendix II

DERIVATION OF STRESS DISTRIBUTION FOR THE SPECIMEN SHOWN IN FIG. 11(c) OF THE TEXT

In this appendix, a differential equation for the fibre axial stress will be derived for the specimen shown in Fig. 11(c) in the text. It is assumed that the axial load carrying capacity of the matrix concentrates in a ring of distance R^* from the fibre centre. The matrix from r_f to R^* carries shear stresses only.

With the coordinate axes defined as in Fig. 11(c), in the matrix, from r_f to R^*,

$$\partial\tau_{rz}/\partial r + \tau_{rz}/r = 0 \tag{34}$$

$$\tau_{rz} = G_m\,\partial w/\partial r \tag{35}$$

where G_m is the shear modulus of the matrix and w is the displacement in the z direction.

Putting $w = u_{R^*}$ at $r=R^*$ and $w=u_f$ at $r=r_f$, and integrating from r_f to R^*, we have:

$$\tau_f = \tau_{rz}\,|_{r=r_f} = G_m(u_{R^*} - u_f)/[r_f\log(R^*/r_f)] \tag{36}$$

Equilibrium of fibre stress and interfacial shear stress requires that:

$$\partial\sigma_f/\partial z + (2/r_f)\tau_f = 0 \tag{37}$$

Global equilibrium requires that:

$$V_f\sigma_f + V_m\sigma_m = V_m(V_f\sigma_p/V_m) = V_f\sigma_p \tag{38}$$

where σ_f and σ_m are the fibre and matrix stresses respectively and $(V_f\sigma_p/V_m)$ is the applied stress at the surface of the matrix.

Also, from strain–displacement relations:

$$\partial u_f/\partial z = \sigma_f/E_f;\ \partial u_{R^*}/\partial z = \sigma_m/E_m \tag{39}$$

Combining Equations (36)–(39), we have:

$$\partial^2\sigma_f/\partial z^2 - (\rho/r_f)^2\sigma_f = -(\rho/r_f)^2\,\alpha\sigma_p \quad (40)$$

ρ and α have been defined in the text.

The boundary conditions are:

$$\sigma_f = 0,\ z = 0$$
$$\sigma_f = 0,\ z = L \quad (41)$$

On solving, we have

$$\sigma_f = \alpha\sigma_p \{ 1 - \cosh(\rho z/r_f) - [1 - \cosh(\rho L/r_f)] \sinh(\rho z/r_f) / \sinh(\rho L/r_f) \quad (42)$$

$$\tau_f = (\rho/2)\,\alpha\sigma_p \{ \sinh(\rho z/r_f) + [1 - \cosh(\rho L/r_f)] \cosh(\rho z/r_f) / \sinh(\rho L/r_f)\} \quad (43)$$